

## First results of the THEMIS Search Coil Magnetometers

O. Le Contel · A. Roux · P. Robert · C. Coillot ·  
A. Bouabdellah · B. de la Porte · D. Alison ·  
S. Ruocco · V. Angelopoulos · K. Bromund ·  
C. C. Chaston · C. Cully · H. U. Auster · K. H.  
Glassmeier · W. Baumjohann · C. W. Carlson · J.  
P. McFadden · D. Larson

Received: date / Accepted: date

**Abstract** We present the first data from the THEMIS Search Coil Magnetometers (SCM), taken between March and June 2007 while the THEMIS constellation apogee moved from the duskside towards the dawnside. Data reduction especially the SCM calibration method and cleanup process are described. The signatures of magnetic fluctuations in key magnetospheric regions such as the bow shock, the magnetopause and the magnetotail during a substorm, are described. We also discuss the role that magnetic fluctuations could play in plasma transport, acceleration and heating.

**Keywords** First keyword · Second keyword · More

---

O. Le Contel · A. Roux · P. Robert · C. Coillot · A. Bouabdellah · B. de la Porte · D. Alison · S. Ruocco  
Centre d'étude des Environnements Terrestre et Planétaires (CETP), 10-12 avenue de l'Europe, F-78140  
Vélizy, France  
Tel.: 33-1-39254945, Fax: 33-1-39254922  
E-mail: olivier.lecontel@cetp.ipsl.fr

V. Angelopoulos  
Space Sciences Laboratory, University of California, Berkeley, CA, USA

K. Bromund  
SP Systems, Inc. on contract to NASA/GSFC, Space Weather Laboratory, Code 674, Greenbelt, MD, USA

C. C. Chaston  
Space Sciences Laboratory, University of California, Berkeley, CA, USA

C. Cully  
Laboratory for Atmospheric and Space Physics, University of Colorado, Boulder, CO, USA

H. U. Auster · K. H. Glassmeier  
Institut für Geophysik und extraterrestrische Physik der Technischen Universität Braunschweig, D-38106  
Braunschweig, Germany

W. Baumjohann  
Space Research Institute, Austrian Academy of Sciences, Graz, Austria

C. W. Carlson · J. P. McFadden · D. Larson  
Space Sciences Laboratory, University of California, Berkeley, CA, USA

## 1 Introduction

The identification of the instability leading to substorm breakup and expansion is a key issue for magnetospheric physics and beyond. Indeed similar explosive processes are known to occur in other astrophysical contexts, such as the solar corona, and in laboratory machines designed to control the fusion. In all cases the accumulated magnetic energy is released explosively, thereby leading to fast changes in the magnetic configuration and to particle acceleration. These plasmas being hot and dilute, binary collisions are rare and cannot ensure the dissipation requested for the development of instabilities leading to break the configuration, such as the collisionless tearing instability. Kinetic effects, in particular associated with the development of waves, are expected to take over the role that binary collisions cannot ensure. Together with the Electric field Instrument (EFI) [4] THEMIS Search Coil Magnetometer (SCM) will be used to identify the possible role of waves at substorm breakup, and expansion phase. It will also allow a remote tracking of the motion of active regions, via ducted waves. The association between substorm onset and intense emissions of ULF/ELF/VLF waves has been known for quite a long time [8, 29, 9]. Later, the search coils magnetometers onboard the geostationary european satellite GEOS-2, launched in 1978, detected magnetic impulsive signals in the range 0.5 - 11.5 Hz (ULF) at substorm breakup [27], characterized by particle injection and changes from a taillike to a more dipolar magnetic configuration. Robert et al. interpreted the Short Irregular Pulsations (SIPs) observed at breakup as the signatures of small scale field aligned current structures passing by the spacecraft [27]. Due to their non steadiness these structures can also be interpreted as kinetic Alfvén waves in the proton gyrofrequency (0.1-1 Hz) range [24]. Kremser et al. showed that electron parallel acceleration takes place inside these structures [12]. On the basis of AMPTE/CCE data ( $X_{GSM} \simeq -8.8 R_E$ ) Lui et al. suggested that the cross field current driven instability triggers substorm onset [19, 18]. Farther in the magnetotail ( $X_{GSM} \simeq -15.2 R_E$ ), observations from the japanese Geotail satellite give evidence for the existence of electromagnetic waves in the lower hybrid frequency range during a small substorm [31]. Yet the authors concluded that wave energy is too small to supply enough dissipation, via anomalous resistivity, to allow a resistive mode instability to develop. On the theoretical side, Cheng and Lui proposed another solution to resolve substorm onset enigma; they suggested that the coupling between high frequency (cross tail current instability) and low frequency (ballooning modes) electromagnetic fluctuations accounts for the fast occurrence of the breakup onset [6]. As the Geotail apogee moved closer to the earth ( $X_{GSM} \simeq -10$  to  $-13 R_E$ ), magnetic fluctuations were also observed during substorm in the proton gyrofrequency (0.1-1 Hz) range as well as in the lower hybrid frequency range (5-16 Hz). However, according to Sigsbee et al. these fluctuations reach their maximum amplitude after onset and could not therefore be considered as a substorm trigger [35]. Further analysis of GEOS-2 data (at the geostationary orbit) suggested that substorm onset and impulsive plasma transport is controlled by a micro-instability with frequencies around the proton gyrofrequency such a parallel current instability [22, 23, 13, 14]. The regular occurrence, at different radial distances (at the geostationary orbit with GEOS-2, at  $10 R_E$  with Geotail and  $20 R_E$  with Cluster) of wave activity around the proton gyrofrequency, at substorm onset, was also noted by Le Contel et al. [15]. Yet more recent analysis of Geotail observations in the near-earth plasma sheet ( $X_{GSM} \simeq -8.3 R_E$ ) gave evidence for large amplitude wave emissions (5-15 nTs<sup>-1</sup>) in the lower hybrid frequency range (5-20 Hz), just prior to the dipolarization [32]. Thus the identification of the intense waves that develops at substorm onset, and the elucidation of their potential role at triggering breakup, is still a matter of debate. In this context the determination of the radial distribution of wave characteristics is an important issue that should be

resolved thanks to THEMIS wave instrumentation. THEMIS orbit is well suited to achieve this goal [1, 33], but one has to realize that the full characterization of the waves is made difficult by the rapid changes of the magnetic configuration during substorm and by the strong inhomogeneity of the medium. In order to avoid adding confusion in the debate it would be wise to use the same parameter namely the amplitude  $B$  of the waveform, rather than its derivative ( $\omega B$ ). Indeed the use of the derivative can give the false impression that amplitudes are larger at larger frequencies. At higher frequencies, whistler waves were identified in the magnetotail and proposed as a way to monitor energetic electrons and processes of reconnection [36]. More recently Cluster observations from the STAFF instrument [7] gave evidence for very large amplitude ( $\simeq 1$  nT) waves in the whistler mode range ( $f_{ci} < f < f_{ce}$ ), emitted in the magnetotail during substorms [16]. These intense emissions last only a few seconds and are associated with very thin current sheets ( $\leq \rho_i$ , the proton Larmor radius). They occur in conjunction with accelerated electrons. Whistler mode waves are expected to be produced in some of the magnetic reconnection theories [20]. Yet, at present time, it is unclear whether they are a by-product of reconnection or they effectively play a crucial role as a trigger of the substorm process. Further studies are therefore needed in order to clarify the role of these different kinds of wave during various substorm phases. Substorm is not the only space physics process for which waves could play a crucial role. Magnetic reconnection and plasma transport at the magnetopause can be modelled as a global process controlled by the level of ULF wave activity (see for instance [26]). Magnetosheath turbulence is fundamentally based on mirror mode wave activity [30]. Dissipative mechanisms for collisionless shock are thought to be also strongly related to wave activity [11]. Therefore THEMIS SCM instruments not only should gather crucial data for substorm studies but also for all the main fundamental processes controlling the physics of collisionless plasmas, namely shock, magnetic reconnection, turbulence, plasma acceleration, transport and heating. In section 2 we briefly present the science objectives and measurements requirements also detailed in a companion paper [28]. Section 3 is devoted to the presentation of the data reduction especially the calibration and cleanup processes needed for a scientific use of SCM data. Preliminary science results are discussed in section 4 for different regions, from the solar wind to the magnetotail, via magnetosheath and magnetopause.

## 2 Science objectives and measurement requirements

The primary goal of the Time History and Macroscale Interaction during Substorms (THEMIS) mission is to establish when and where do substorms start, and to use this information to resolve the controversy about what instability triggers substorms [1]. The main difference between the two types of models is the sequence of events that leads to the breakup. For the first type of models, magnetic reconnection (MR), presumably associated with the development of the tearing instability, is what triggers substorms. In the second type of model, labelled as ‘‘Current Disruption’’ or CD, the breakup is triggered by a reduction in the cross-tail current, associated with the development of an instability. In both cases ULF and ELF waves are expected to play a critical role. In recent versions of the MR models [20] whistler mode waves are expected to accelerate electrons up to very large (super-Alfvénic) velocities, thereby enhancing the reconnection rate. It has also been suggested [5, 2] that very thin current sheets can be destabilized directly by HF tearings in the whistler mode range. On the other hand, in CD models the cross tail current can be directly disrupted by HF cross field instabilities, or undergo low frequency (ballooning modes) instability coupled via  $\text{div}J=0$ , to parallel currents, which eventually drives ion cyclotron and/or whistler mode instabilities.

**Table 1** Matrices of rotations: Matrix **U2G** from Sensor mechanical coordinates (SMC) to probe geometric coordinates (SPG); Matrix **G2S** from Probe geometric coord. (SPG) to probe spin-Sun sensor coord. (SSL)

U2G			G2S		
0.9777	-0.2100	0.00000	-0.7071	0.7071	0.0000
0.2100	0.9777	0.00000	-0.7071	-0.7071	0.0044
0.0000	0.0000	1.00000	0.0031	0.0031	1.0000

The modelling of the latter instabilities is made difficult by the fact that electron bounce frequency in the magnetotail is around the proton gyrofrequency. Therefore the proper handling of HF frequency current driven instabilities should take into account the electron bounce motion and the corresponding electron bounce resonance [10]. Thus the identification of the waves, at substorm breakup (and during the expansion phase), is an important clue towards understanding what triggers substorms. Together with the EFI instrument, which measures electric fields in the same frequency range, the Search Coil Magnetometer (SCM) will determine the nature of the waves that develop at breakup and during the expansion phase and, in the case of guided waves, help tracking remotely the active region where breakup starts. SCM is also needed to assess whether waves are electrostatic (such as lower hybrid waves) or electromagnetic (such as whistler mode waves). Thus wave observations provide a critical test to substorm scenarios and could provide a remote sensing of substorm dynamics during the expansion phase.

### 3 Data reduction

#### 3.1 Reminder on THEMIS coordinate systems

Raw data are recorded in the sensor magnetic coordinate system for which axis are defined by magnetic axis of search coils (see also [28]). Figure 1 displays the SCM antennas at the tip of the boom and gives different angles between antenna axis and probe geometric axis. In order to express data in geophysical frame such as the GSE we need to perform the following coordinates transformations associated with the application of rotation matrices (see for more details [25]):

(1) Data are moved from sensor magnetic coordinate system to sensor mechanical coordinate system (SMC); actually these frames can be considered as identical.

(2) Then data are moved from this latter frame to the spinning probe geometrical coordinate system (SPG) for which X axis corresponds to the ProbeX axis (see figure 1) and Z axis is along the geometric Z axis (U2G matrix, see table 1), the origin being at the geometric probe center.

(3) Then from SPG frame to the spinning sunsensor L-vectorZ (SSL) coordinate system, for which X is directed toward the sun and the Z axis along the spin axis (G2S matrix, see table 1).

(4) Finally, data are moved into a non spinning system named Despun Sun L-vectorZ (DSL) coordinate system obtained by a rotation about the spin axis by an angle equal to the opposite of the spin phase in the direction of the spin; X axis directed toward the sun and Z axis corresponds to the spin axis.

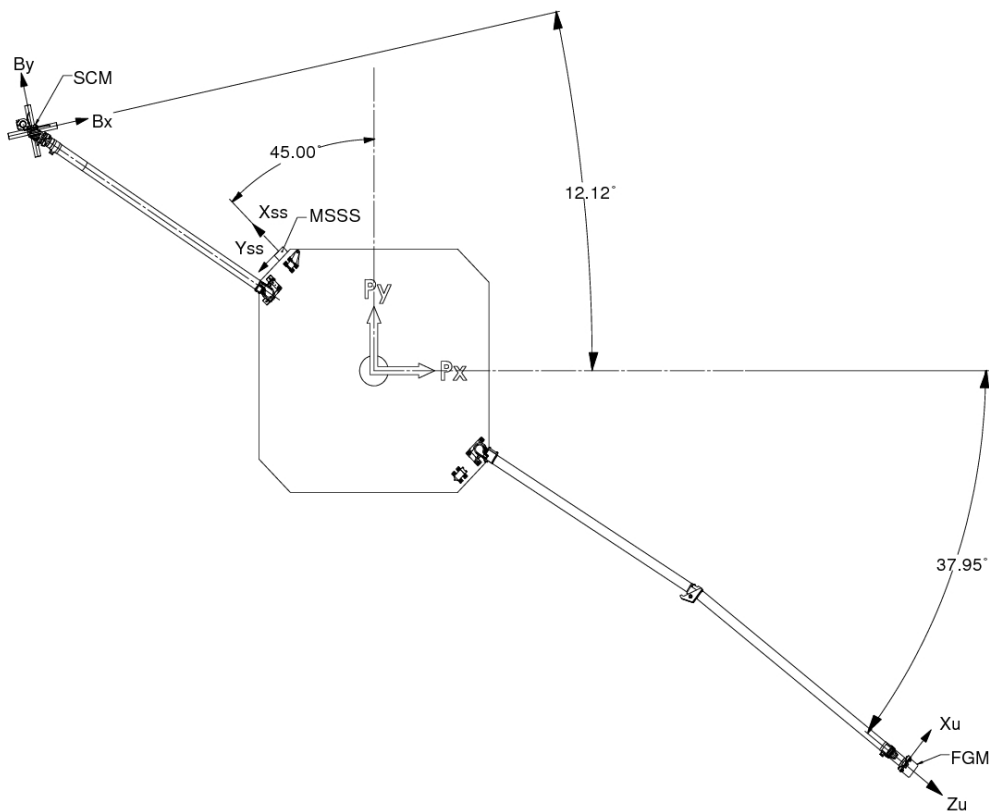


**Fig. 1** Detail of sun sensor coordinates from SSL/UCB

### 3.2 SCM calibration method

Signal in physical units (nT) is obtained by calibration of the raw signal in Volts. Each antenna response is characterized by its own transfer function, giving the ratio V/nT for a given frequency (for more details see [28]). These functions being not linear according to the frequency, a dedicated process must be applied to calibrate the raw waveforms. Basically it exists two methods of calibration:

(1) Perform the Fourier Transformation (FT) of the signal, on a given time period, then divide by the complex transfer function to take into account amplitude correction and phase shift; note that one has to fix a lower cut off frequency  $f_c$  as the transfer function goes to zero at null frequency. Finally perform an inverse FT to get the calibrated signal in time domain.

(2) Convolute the signal with the impulsional response of the transfer function, on a similar time period.

The second method is implemented in the SCM calibration routine of the THEMIS software package; this method permits to use the optimized IDL routine of convolution and gives better results in terms of computing time. The convolution is performed using a sliding window in order to provide a continuous process of calibration.

Calibration of SCM mounted onboard a spinning spacecraft with a spin frequency in the antenna bandwidth such as THEMIS probes requires additional steps compared with

laboratory calibration. Indeed the components of the DC magnetic field perpendicular to the spin axis are measured as a sinusoid with a large amplitude at the spin frequency. Since this DC field ( $\simeq 100$  nT) is about 100 times larger than the wave amplitude ( $\simeq 1$  nT), it has to be removed from the raw signal before calibration to avoid undesirable effects. Furthermore spinning motion at  $f_s$  introduces Doppler shift effect: a circular wave at frequency  $f_L$  turning in the opposite direction of the satellite is measured by the sensor as a wave at frequency  $f_L + f_s$  whereas a wave turning in the same direction at  $f_R$  is measured as a wave at frequency  $f_R - f_s$ . Therefore the sensors mounted onboard a spinning spacecraft, in the spin plane, are not able to reconstitute fully the fluctuations with frequency around the spin frequency. Indeed any circular waves turning in the same direction than the spin rotation, are not detected because their apparent frequency becomes null. This means also that the sensitivity of the experiment at low frequency depends on the polarization of the waves by respect to the spin axis. Practically it is recommended before analyzing waves in a fixed frame (DSL, GSE, GSM ...) to low-filter the data at a minimum frequency higher than the spin frequency, typically  $f_{min}$  could be fixed to the sum of the spin frequency  $f_s$  and the cut off frequency  $f_c$ .

Therefore we can distinguish different steps in the SCM calibration process which are also described in the header of the THEMIS IDL calibration routine for scm data called `thm_cal_scm` available in the THEMIS software package. These different kind of outputs can be obtained using the following values of the step keyword:

**step 0:** *waveform in counts unit*

Each data gap is time tagged and a NaN symbol (Not a Number) are inserted for proper plotting. This step corresponds to raw data expressed in telemetry unit.

**step 1:** *waveform in Volts, spinning sensor system, with DC field*

Conversion factor from telemetry unit to volts is applied to the data but the spin modulation is still present.

**step 2:** *waveform in Volts, spinning sensor system, without DC field*

By using a sliding window of about two spin periods, we estimate the amplitude and phase of the spin signal on the three (x,y,z) components of the signal delivered by the sensors; the x-y amplitude and phase provides a measurement of the component perpendicular to the spin axis of DC magnetic field. This DC magnetic field can be expressed in the DSL system and can be compared to the FGM data, while the amplitude along Z allows the computation of the misalignment angle between the Z sensor axis and the spin axis. Note that the number of spin periods used for the sliding window can be fixed by the `n_spinfit` keyword. At this step, these DC field components are removed from the signal. Furthermore, a special detrend method can be applied to perform a more efficient rejection of the spin signal and its harmonics, but frequency below the detrend frequency are strongly reduced. This treatment can be applied using the `Fdet` keyword that allows to fix the detrend frequency. Finally during this step, a special cleanup method can be also applied to reject some spurious tones coming from the spacecraft and characterized during the commissioning. The cleanup process is described in the next subsection.

**step 3:** *waveform in nT, spinning sensor system, without DC field*

Calibrated waveform for which the DC magnetic field variation has been removed. Note that data are still in a spinning frame associated with the sensors. The calibration is performed using a convolution kernel with a number of points fixed by the `nk` keyword. The choice of the value of `nk` involves a trade-off between quality of the low-frequency calibration and speed of the data processing. By default, an optimal value is chosen for each of the data modes, as a multiple of the sample frequency. For fast survey mode

(scf mode with  $f_e=8$  S/s nominally, where  $f_e$  is the sampling frequency),  $n_k=8*f_e$ . For particle burst mode (scp mode with  $f_e=128$  S/s nominally),  $n_k=4*f_e$  and for wave burst mode (scw mode with  $f_e=8192$  S/s nominally),  $n_k=f_e$ . The  $m_k$  keyword can be used to select a different multiple of the sampling frequency.

**step 4:** *waveform in  $nT$ , spinning SSL system, without DC field*

Same as step 3 but now data are in the SSL system using matrix of table 1.

**step 5:** *waveform in  $nT$ , fixed DSL system, without DC field, filtered*

Data are now calibrated, without DC magnetic field variations and projected in a fixed frame common to all instruments (DSL). After this step SCM waveform can be transformed into any physical frame (GSE, GSM, ...) using cotrans routine available in the THEMIS software package. Note that after coordinates transformations the three original components will be mixed. Therefore it is important to ensure that before the change of frame the parallel and perpendicular components to the spin axis have undergone the same level of filtering. Thus at this step it is recommended to low-filter the three components with the same minimum frequency ( $f_{min}$  being fixed also as a keyword).

**step 6:** *waveform in  $nT$ , fixed DSL system, with  $xy$  DC field*

Same as step 5 but the calculated DC magnetic field components perpendicular to the spin axis are added to the waveform. X-Y components can be compared to the FGM data for cross-calibration. Z component is unchanged.

### 3.3 Cleanup process

First data analysis during commissioning showed that two types of noise with unexpectedly high amplitudes were present on SCM waveform data. First the power system produces a tone at twice the spin frequency (1/3 Hz) and its harmonics. As expected the level of these tones decreases during eclipse period. Secondly, tones at 8 and 32 Hz, and their harmonics, were found to dominate the spectrum at higher frequencies. The frequencies of these tones correspond to the frequencies of instrument clocks onboard the spacecraft. At the present time it has not been possible to identify the exact source of these spurious noise. However we know that the 8 and 32 Hz are due to radiated noise, as their levels strongly decreased after SCM boom deployment (-10 dB). Fortunately both type of spurious noises are locked in phase and relatively constant in amplitude. Spin tones are spinphase locked whereas 8/32 Hz tones are 1s phase locked (C. Cully, private communication). Thanks to this property it was suggested to perform a superposed epoch analysis (SEA) in order to reduce the level of these two types of phase locked noise (C. Chaston; private communication). Therefore a cleanup process was developed based on two successive SEA. SEA consists of cutting the waveform data of duration  $T$  into  $N$  windows of definite duration ( $t_w \ll T$ ), named hereafter averaging windows. These  $N$  windows are superposed, or summed, which gives an average profile of the phase locked noise. Then a "noise waveform" of duration  $T$  is built by duplicating  $N$  times the averaged noise. Finally the noise waveform is subtracted in phase to the raw waveform. The cleanup process can be summarized as: (1) a first SEA with an averaging window equal to a multiple of the spinperiod, (2) a second SEA with an averaging window equal to a multiple of 1s. The cleanup process has been implemented in the current THEMIS software; two versions of the cleanup routine are available and can be activated (or not) in the classic SCM routine by fixing the keyword `clnup_author` (`clnup_author = 'ole'` by default or can be 'ccc'). Basically they give same results but algorithms are slightly different (see code sources for more details). Different levels of cleanup can be selected for each version by using specific keyword (`cleanup = 'spin'` for only spin tones cleanup or 'full' for spin tones

and 8/32 Hz cleanup). Note that the duration in seconds of the first and second averaging windows can be fixed by the keywords `wind_dur_spin` and `wind_dur_1s` respectively. Figure 2 displays the different stages of the cleanup process during a particle burst mode period (scp mode with 128 S/s). Note that some spikes remain after the cleanup process. They come from some noise which is not phase locked therefore SEA does not permit to get rid of them. Figure 3 displays spectra performed from SCM wave burst data (scw mode with 8192 S/s) on March 23rd 2007 between 135945 and 140216 UT. Data are despinned and projected into the sensor coordinates system in order to be compared with data measured at the laboratory. As in the example of figure 2 8/32 Hz tones are strongly reduced by cleanup process but still present in the spectra as other spikes which are not phase locked. However, we see that these in flight measurements give the same Noise Equivalent Magnetic Inductions (NEMI) as reported in [28]:  $0.4 \text{ pT}/\sqrt{\text{Hz}}$  at 10 Hz,  $0.08 \text{ pT}/\sqrt{\text{Hz}}$  at 100 Hz for Bz and 0.15 for Bx and By and  $0.01 \text{ pT}/\sqrt{\text{Hz}}$  at 1 kHz. In flight NEMIs can be smaller than NEMIs at laboratory if in flight temperatures of preamplifiers as well as of sensors are lower than at laboratory (273 deg K). Note that the higher level of noise on Bx and By between 15 Hz and 1 kHz is found to be only on Bx in SSL frame. Therefore this noise is related to the sun sensor direction [17].

## 4 Science results

In this section we present from the solar wind to the magnetotail first examples of THEMIS data.

### 4.1 Solar wind - magnetosheath - dayside magnetosphere regions: June 21st 2007 event

Figure 4 shows the positions in the GSE frame of the THEMIS constellation on June 21st from 0800 to 1050 UT. Around 0800 UT, Tha is the farthest probe from the earth whereas Thb is the closest one; probes c, d and e are slightly separated along Y but almost at the same X in between a and b. The selected time period corresponds to a fast survey mode. In this mode FGM data [3] have 0.25 sec time of resolution (panels a,b,c and d). Ion ESA data [21] including moments ( $n_i$ ,  $V_i$ ,  $T_i$ ) have 3 sec time of resolution (panels e,f,g, and h), electron fluxes are available with the same time resolution (panel i). SCM waveform data have 0.125 sec time of resolution (scf mode) whereas spectra time resolution is 32 sec (panels j,k,l, and m). For most of the selected time period Tha is located in the solar wind as illustrated by figure 5. Indeed from 0800 to 1015 UT, the magnetic field modulus is smaller than 10 nT (panel d), the average ion energy is around 800 eV (panel e) with  $n_i \simeq 10 \text{ p}\cdot\text{cm}^{-3}$  (panel f),  $V_x \simeq -350 \text{ km}\cdot\text{s}^{-1}$  (panel g) and  $T_i \leq 50 \text{ eV}$  (panel h). Average electron energy (panel i) is no more than 15 eV which is consistent with the characteristics of the slow solar wind around 1 astronomical unit. At 1015 UT Tha crosses the shock as the modulus of B increases from 5 to 15 nT, the  $V_x$  component of the ion velocity decreases from 400 to 150  $\text{km}\cdot\text{s}^{-1}$ , the ion density increases from 10 to more than 40  $\text{p}\cdot\text{cm}^{-3}$  and the ion temperature increases from less than 70 eV to more than 200 eV. Therefore the solar wind slows down and is heated as it goes through the collisionless shock. The amplitude of magnetic fluctuations in the ultra low frequency (ULF) range is maximum at the shock crossing ( $\simeq$  few nT) with frequencies up to (at least) 4 Hz, while it is less intense ( $\leq 1 \text{ nT}$ ) and mainly below 1 Hz in the magnetosheath after 1014 UT. In addition to the shock crossing described above, wave and ESA data give evidence for smaller perturbations (0825, 0850, 0925 and 1000 UT) which look like as very

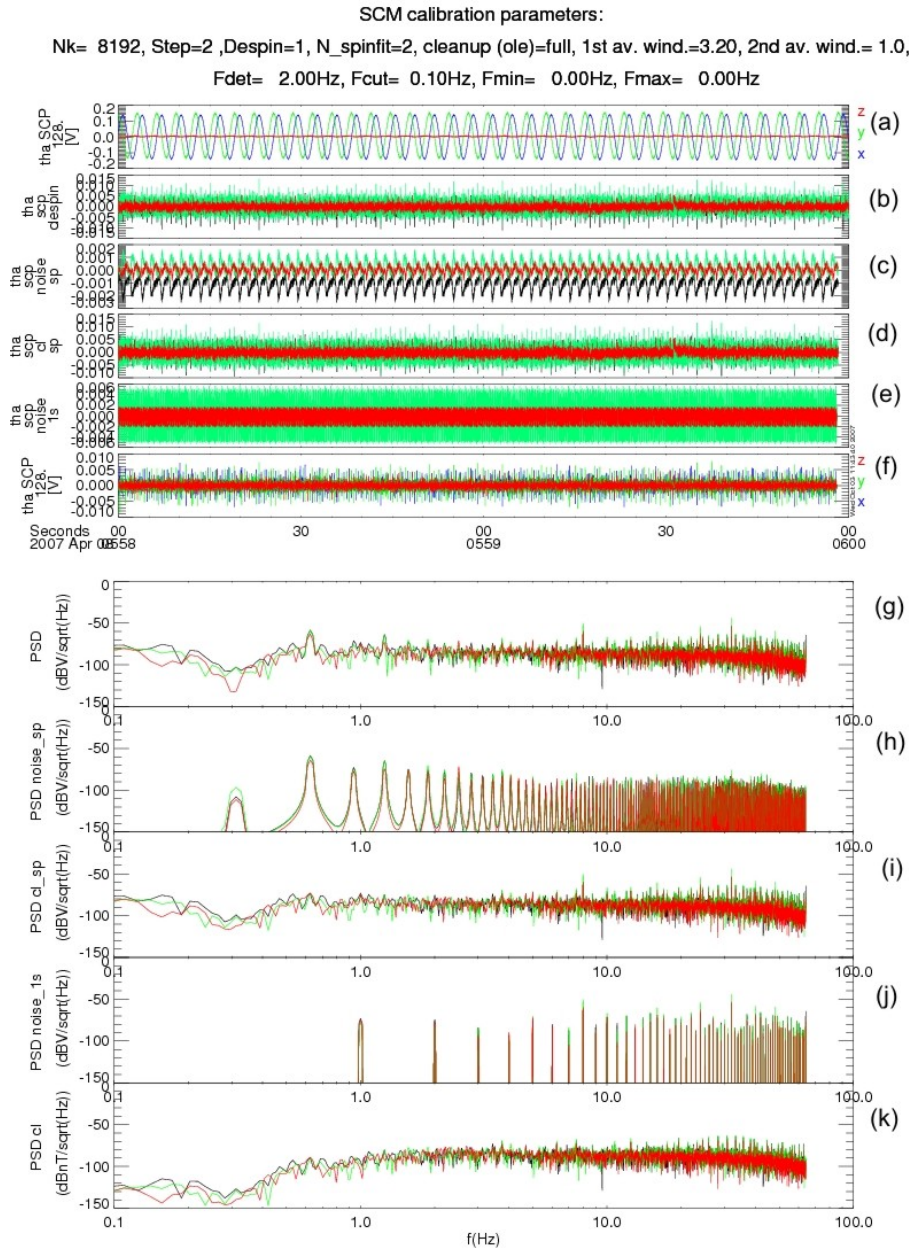


**Fig. 2** scp data recorded by Tha on April 8th, 2007 between 0558 and 0600 UT. From top to bottom: (a) scm raw waveform in volts, (b) despinned waveform, (c) spin phase locked noise built by applying SEA, (d) cleaned (only power ripples) waveform, (e) 1s phase locked noise waveform (SEA), (f) fully cleaned waveform, corresponding spectra in  $\text{dBV}/\sqrt{\text{Hz}}$  follow in the same order except for despinned waveform data: (g) spectrum of (b), (h) spectrum of (c), (i) spectrum of (d), (j) spectrum of (e), and (k) spectrum of (f). Tones at  $2f_s$ ,  $4f_s$ , 8 and 32 Hz are strongly reduced. However, note that at the end of cleanup process (panel k) some spikes are still visible at high frequencies due to the fact that they come from noise which is not phase locked

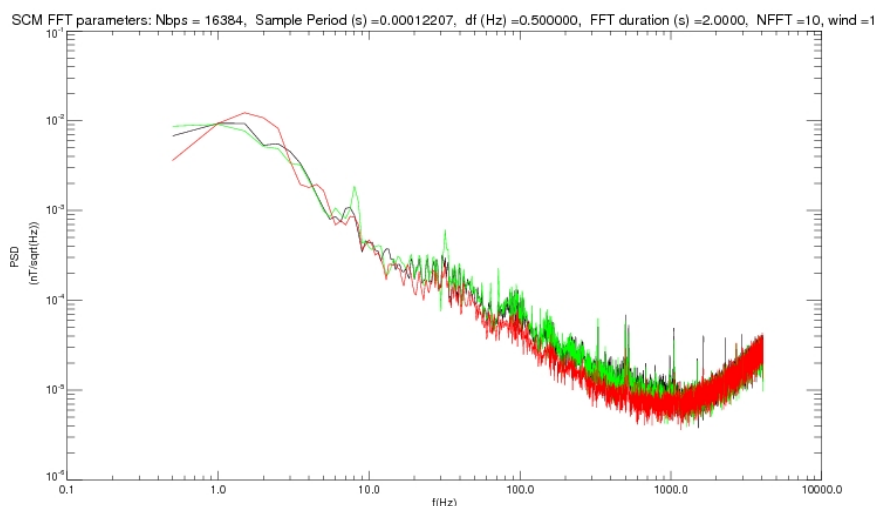


**Fig. 3** Spectra of SCM data during a wave burst period (scw mode) on March 23rd 2007 from 1359:45 to 1400:16 UT. Data are in sensor coordinate system (step 3), with  $n_k = 16384$ ,  $Despin=1$ ,  $Fdet = 2$ . and a full cleanup with  $wind\_dur\_1s=1$ .

brief shock crossing or approach. Notably the sharp signature around 0850 UT has the same characteristic as the shock crossing (velocity decrease, temperature and density increases, strong wave activity up to 4 Hz). It could correspond to a fast sunward then earthward motions of the shock. Unlike the 1050 UT shock crossing, however, energetic ions are also detected together with perturbations, which tells us that the probe penetrates in the foreshock before possibly cross the shock. On figure 6 same set of data, but now gathered by Thb (the closest to the earth) is displayed. Thb is almost always into the magnetosheath during the selected time period excepted between 0920 and 0930 UT when it briefly crosses the shock and after 1020 UT when it enters into the magnetosphere. During the period where probe b is in the magnetosheath the amplitude of ULF magnetic fluctuations varies strongly (panels j,k,l and m); probe b records three intensifications (0825, 0850, and 1000 UT) up to 15 nT well above the average magnetosheath amplitude ( $\leq 1 - 2$  nT) in addition to the intensification associated with the shock crossing at 0925 UT. These intensifications seem to correspond to the small perturbations (1 to 1) observed on Tha data in the solar wind region, and discussed above. Yet the amplitude of the magnetic fluctuations are larger by a factor 5-10 in the magnetosheath and a mechanism of amplification has to be invoked. Also, the magnetopause crossing detected by Thb (1018 UT) turns out to occur four minutes later than the shock crossing detected by probe a (1014 UT) which suggests a sunward global motion of both the magnetopause and the shock. In addition to this global outward motion, quasi-periodic perturbations convected by the solar wind lead to crossing of the ion foreshock and even skimming along the bow shock. Cluster and Geotail are located close to the magnetopause in the dawnside and dusksector, respectively. They detect magnetopause crossings during the same time period. Thus this event is particularly well suited to conduct a global analysis of the shock/magnetopause response to solar wind perturbations.

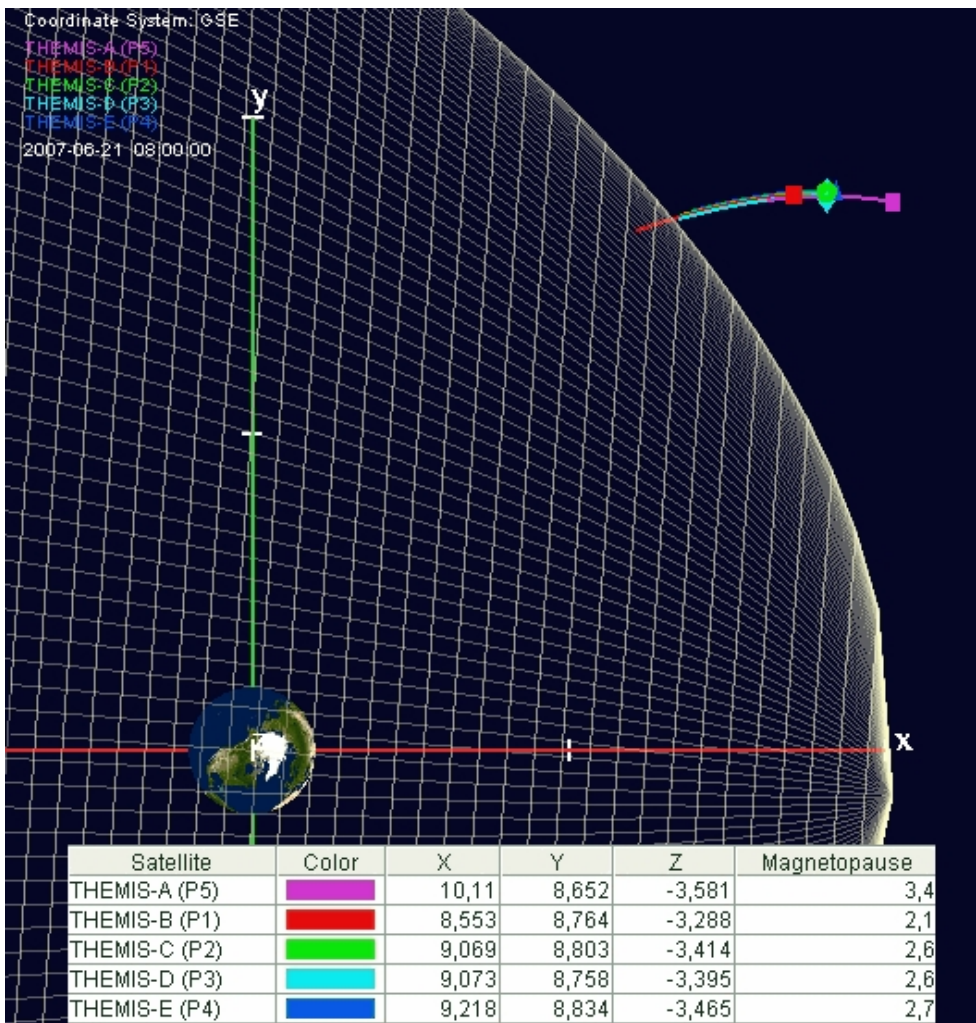


**Fig. 4** THEMIS probe locations (GSE,  $R_E$ ) on June 21st 2007 between 0800 and 1050 UT (This product is available at <http://sscweb.gsfc.nasa.gov/tipsod>). Satellite locations are also tabulated in GSE coordinates at 0800 UT. Magnetopause location for a solar wind dynamic pressure of 3.5 nPa (obtained from WIND survey) is also shown as well as distance to the magnetopause for each probe

#### 4.2 Flux transfer event: May 20th 2007

On May 20th, 2007, the 5 THEMIS spacecraft passed by a FTE. Figure 7 shows the locations of spacecraft in GSE. Notice that Y is of the order of  $12.5 R_E$ , while X is of the order of  $5.5 R_E$ . Thus the satellites were located in the afternoon sector. Spacecraft configuration is particularly interesting since the five satellites bracket the FTE structure, with Thb and Thc on the magnetospheric side, Tha and The on the magnetosheath side, while Thd is close to the magnetopause current layer as illustrated by the estimated distances to the magnetopause of each probe on Figure 7. The geometry of the FTE, and the general characteristics of this event will be discussed elsewhere [33,34]. Here we give a preliminary description

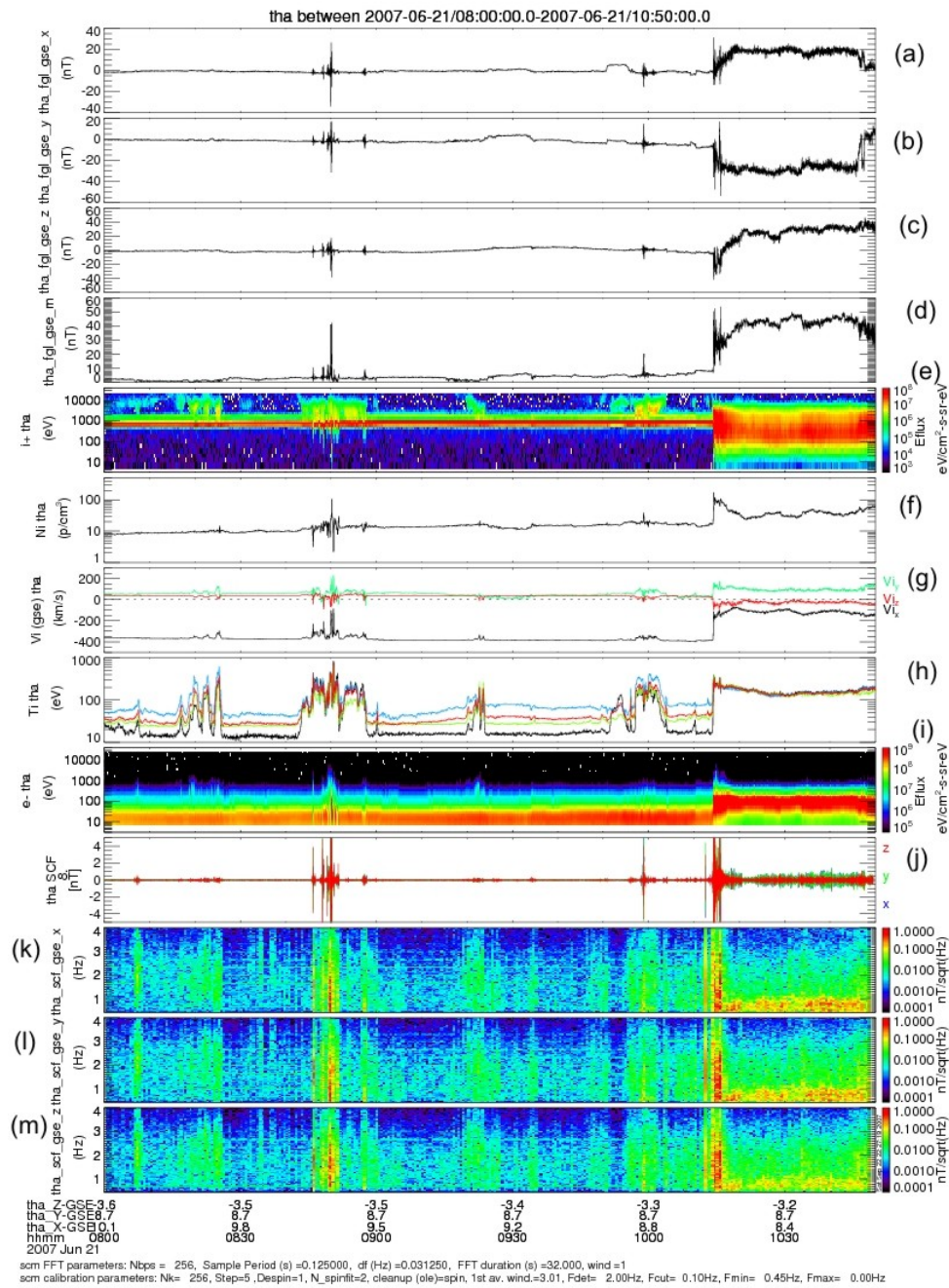


**Fig. 5** From top to bottom: panels a,b,c, and d correspond to Bx, By, Bz and B (FGM data), ion energy spectrogram (panel e), density (f), velocity (g) and temperature (h), panel i corresponds to electron energy spectra (ESA data), panels j,k,l, and m display waveforms and spectrograms of Bx,By and Bz fluctuations from 0.45 to 4 Hz, (SCM data)

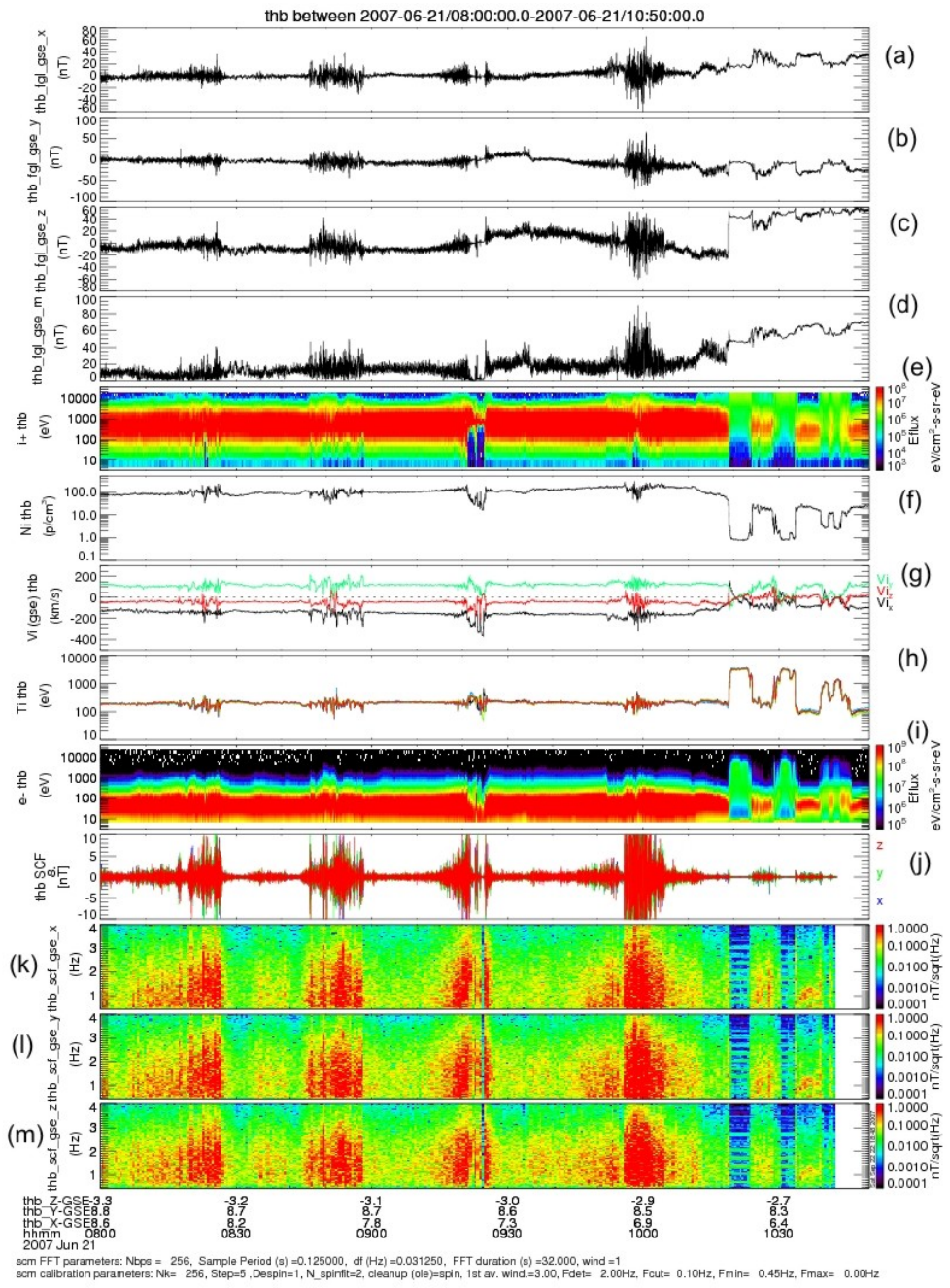
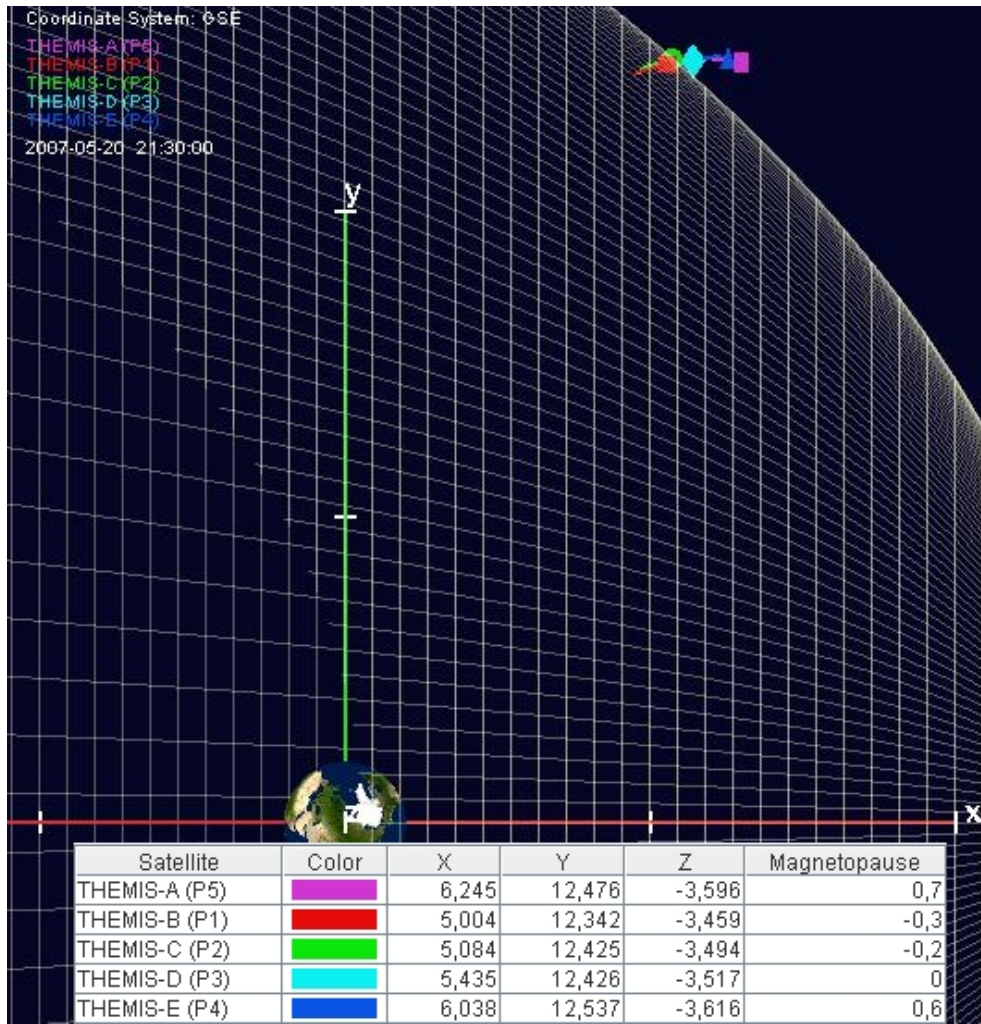


Fig. 6 same legends as Figure 5



**Fig. 7** THEMIS probe locations (GSE,  $R_E$ ) on May 20th 2007 between 2130 and 2230 UT. Satellite locations are also tabulated in GSE coordinates at 2200 UT. Magnetopause location for a solar wind dynamic pressure of 1 nPa (obtained from WIND survey) is also shown as well as distance to the magnetopause for each probe.

of ULF wave observations inside and near the FTE, and suggest possible wave-particle interactions. For practical reasons we only show data from Thc, in Figure 8; data from the other spacecraft are available and commented below. The magnetic structure of the FTE is clearer on Thb, Thc, and Thd, located inside the magnetosphere and at the current layer, than on Tha and The, on the magnetosheath side. Figure 8, panels a, b, and c shows the 3 magnetic components in GSE, while panel d shows the modulus of B. Thc on the magnetospheric side, observes a bipolar magnetic field signature of  $B_y$ , which is close to be normal to the nominal magnetopause. A crater-like variation in the magnetic field strength is observed on Thb, (which is the closest to the earth), and to a lesser extent on Thc (see Figure 8, panel d). On Thd, at the current layer, a maximum in the modulus of B is found. Thc was first in the magnetosphere (before 2201:50), as evidenced by the large energies of electrons

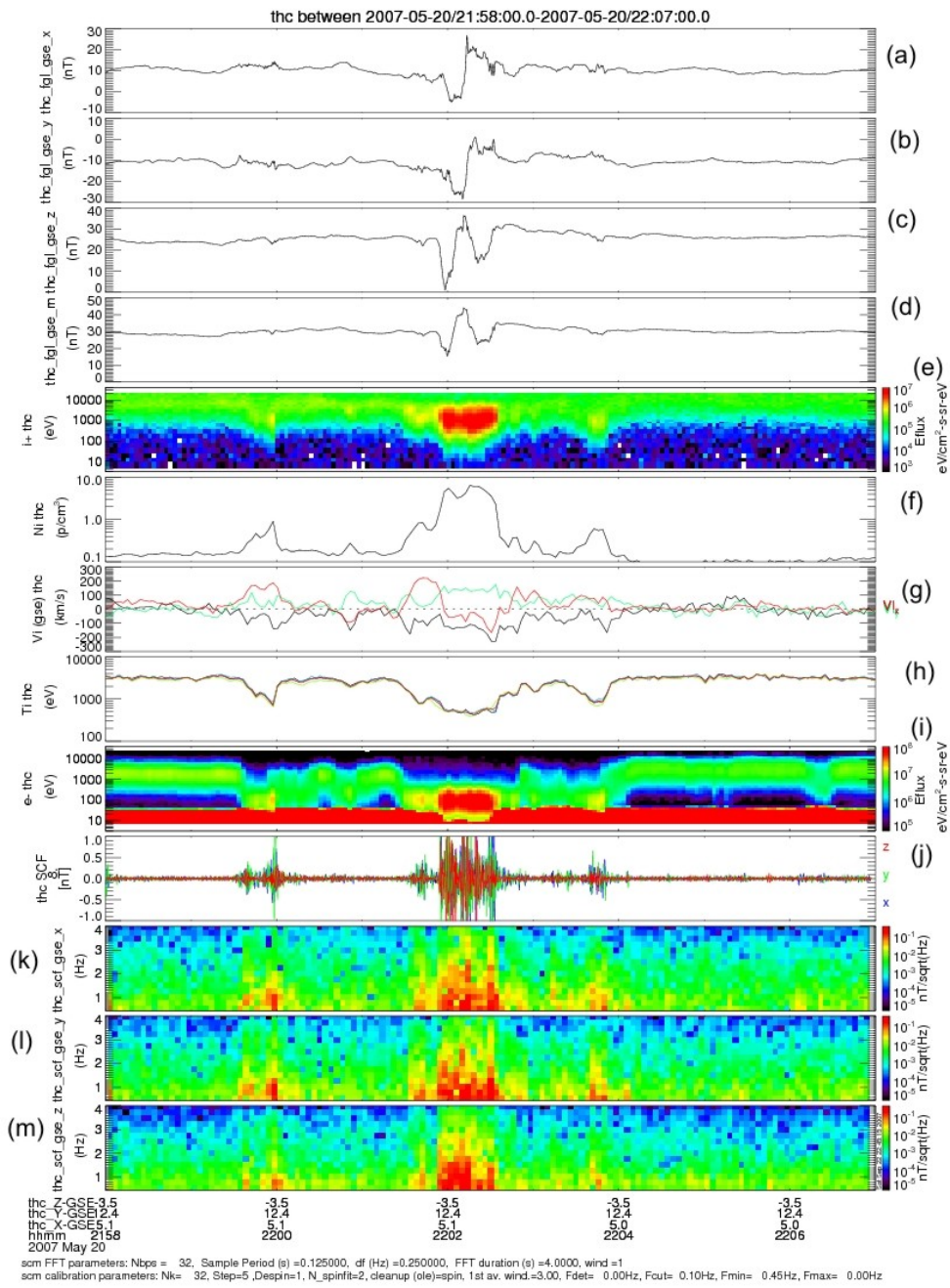
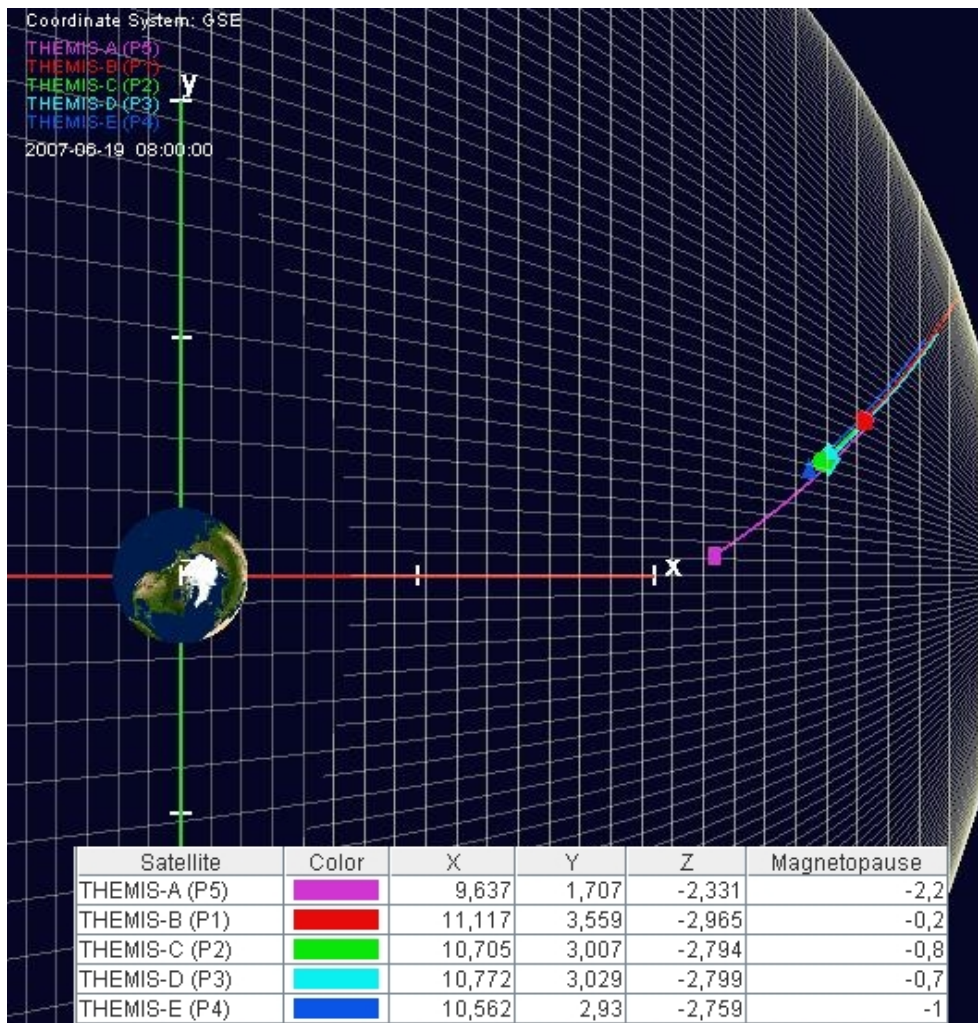


Fig. 8 same legends as Figure 5 but time resolution of spectra is 4 sec

(panel i) and ions (panel e), and it returns to the magnetosphere after FTE crossing (after 2202:30). As it penetrates in the core of the FTE, Thec observes increased ion flux, corresponding to heated magnetosheath plasma (panel e) (ii) enhanced densities, comparable to magnetosheath values (panel f), (iii) enhanced ion flow velocities (panel g), (iv) enhanced fluxes of accelerated or heated magnetosheath electrons (panel i) and (v) enhanced magnetic components of ULF waves (panels j to m). The simultaneity between ULF waves and particle acceleration/heating suggests that a wave-particle interaction process is at work. Can we use data from the other spacecraft to discriminate between possible wave interaction processes; in particular can we identify the particle species, electrons or ions, involved in the interaction with waves? In the magnetosheath The and Tha observe quasi-steady fluxes of magnetosheath ions. The flux and the energy bandwidth do not change as these spacecraft pass by the FTE, and ions are not correlated with variations in wave amplitude. On the other hand magnetosheath electrons (The and Tha), and current sheet electrons (Thd) are also heated/accelerated in a region broader than the FTE, but this region coincides with wave observations. In summary ULF waves are observed together with accelerated/heated electrons. On the magnetospheric side these signatures coincide with that of the FTE, while on the magnetosheath side and at the current layer, ULF waves and heated/accelerated electrons are observed in a broader (boundary layer) region. These preliminary observations suggest that electromagnetic waves interact with electrons, inside the FTE, on the magnetospheric side, and in a broader region comprising the current layer, on the magnetosheath side. We will analyse wave characteristics, as well as the shape of the electron distribution function, and investigate possible signatures of wave particle interactions as a potential electron heating mechanism. More detailed studies based on the analysis of electron distributions are planned to confirm these preliminary results.

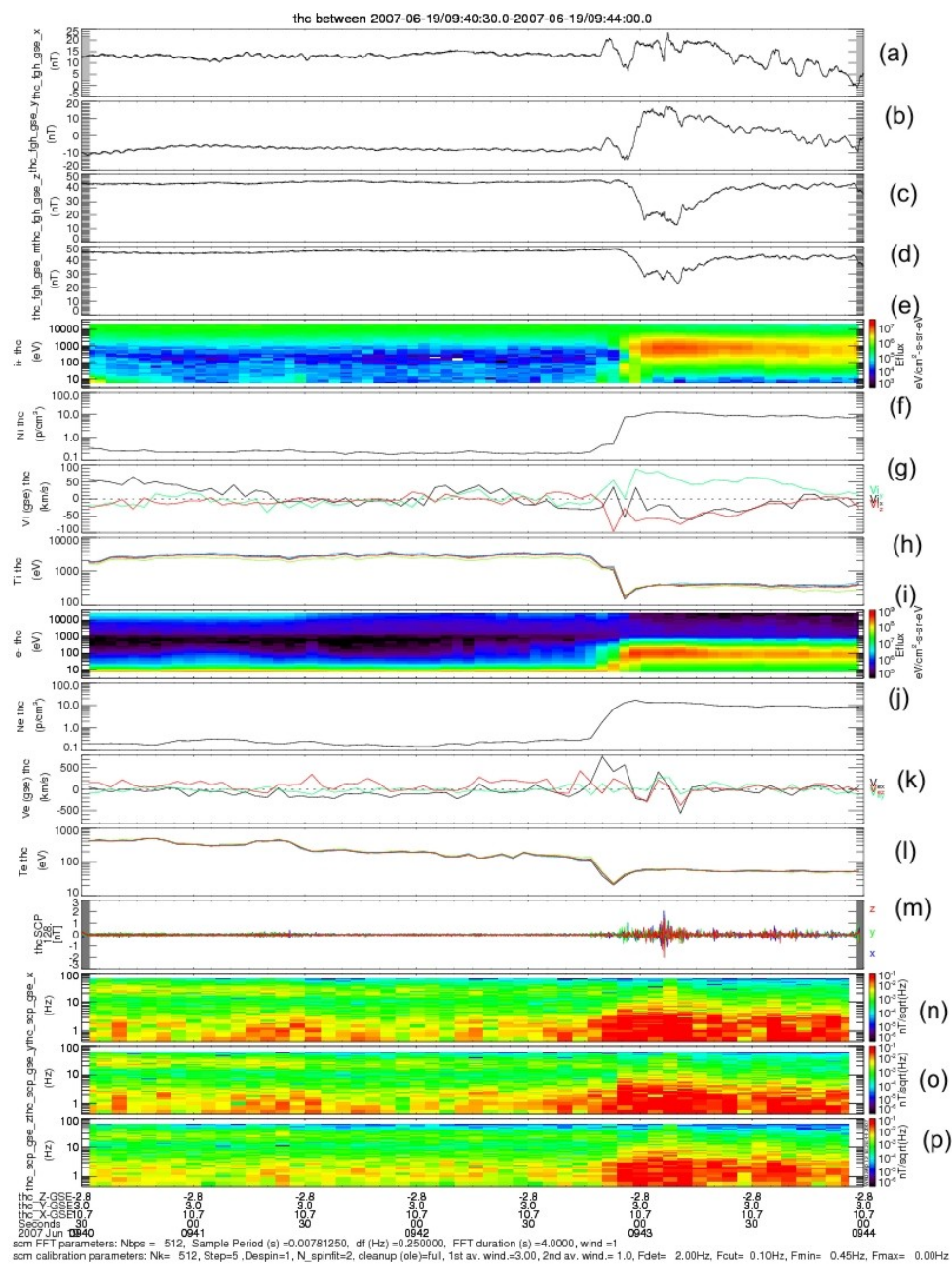
#### 4.3 Magnetopause crossing event: June 19th 2007

Figure 9 displays the THEMIS constellation between 0800 and 1030 UT. Thb is the leading probe while Tha is the trailing one; Thc, Thd, and The follow almost the same trajectory. As the THEMIS constellation goes away from the earth it moves toward the duskside and out of the GSE equator. THEMIS instruments are in the fast survey mode (not shown) during this time period (0800-1030 UT). Gathered data show that Tha is most of the time in the quiet magnetosphere. The other probes leave the magnetosphere to enter the magnetosheath in the following order Thb first then, Thd and Thc almost at the same time and finally The. Before staying definitely in the magnetosheath each probe undergoes multiple magnetopause crossings, hence the timing has to be considered in the averaged sense. Note that Thd and Thc undergo exactly the same number of magnetopause crossings although magnetic field or density profiles can be slightly different thereby indicating a temporal variation of the boundary during its motion. Now we focus on the particle burst period recorded onboard Thc between 0940:30 and 0944:00 UT shown on figure 10. In this mode FGM data are sampled at 128 S/s (panels a,b,c, and d), ion and electron moments from ESA data are available at 3 s time of resolution (panels e to l) and SCM data are sampled at the same rate as FGM (panels m to p). All instrument signatures indicate that Thc crosses the magnetopause and enters into the magnetosheath: the modulus of B decreases (from 45 nT to 30-35 nT), the particles density increases (from 0.2 to 10 p-cm<sup>-3</sup>), while particle temperatures decrease (from 2 keV to 300 eV). The amplitude of the ULF magnetic fluctuations is maximum at the boundary; their frequencies increase up to 10 Hz as the probe crosses the magnetopause. Ion and electron fluxes as well as velocities are maximum within the boundary and during the in-



**Fig. 9** THEMIS probe locations (GSE,  $R_E$ ) on June 19th 2007 between 0800 and 1030 UT. Satellite locations are also tabulated in GSE coordinates at 0943 UT. Magnetopause location for a solar wind dynamic pressure of 1 nPa (obtained from WIND survey) is also shown as well as distance to the magnetopause for each probe.

tense ULF magnetic wave activity. More investigations are needed to know whether plasma transport occurs through the boundary and whether magnetic fluctuations play a crucial role in this transport. In particular electron moments have to be carefully checked in such conditions where the density varies fastly (see [21] for discussion on this instrumental issue). However we can already mention that an amplification of the magnetosheath turbulence at the magnetopause is expected by models and has been already observed by previous magnetospheric missions. Models show that it can lead to a plasma transport across the boundary (see for instance [26]).



**Fig. 10** From top to bottom: panels a,b,c, and d correspond to  $B_x$ ,  $B_y$ ,  $B_z$  and  $B$  (FGM data), ion energy spectrogram (panel e), density (f), velocity (g) and temperature (h), electron energy spectrogram (i), density (j), velocity (k) and temperature (l) (ESA data), panels m,n,o, and p display waveforms and spectrograms of  $B_x$ ,  $B_y$  and  $B_z$  fluctuations from 0.45 to 64 Hz (SCM data)

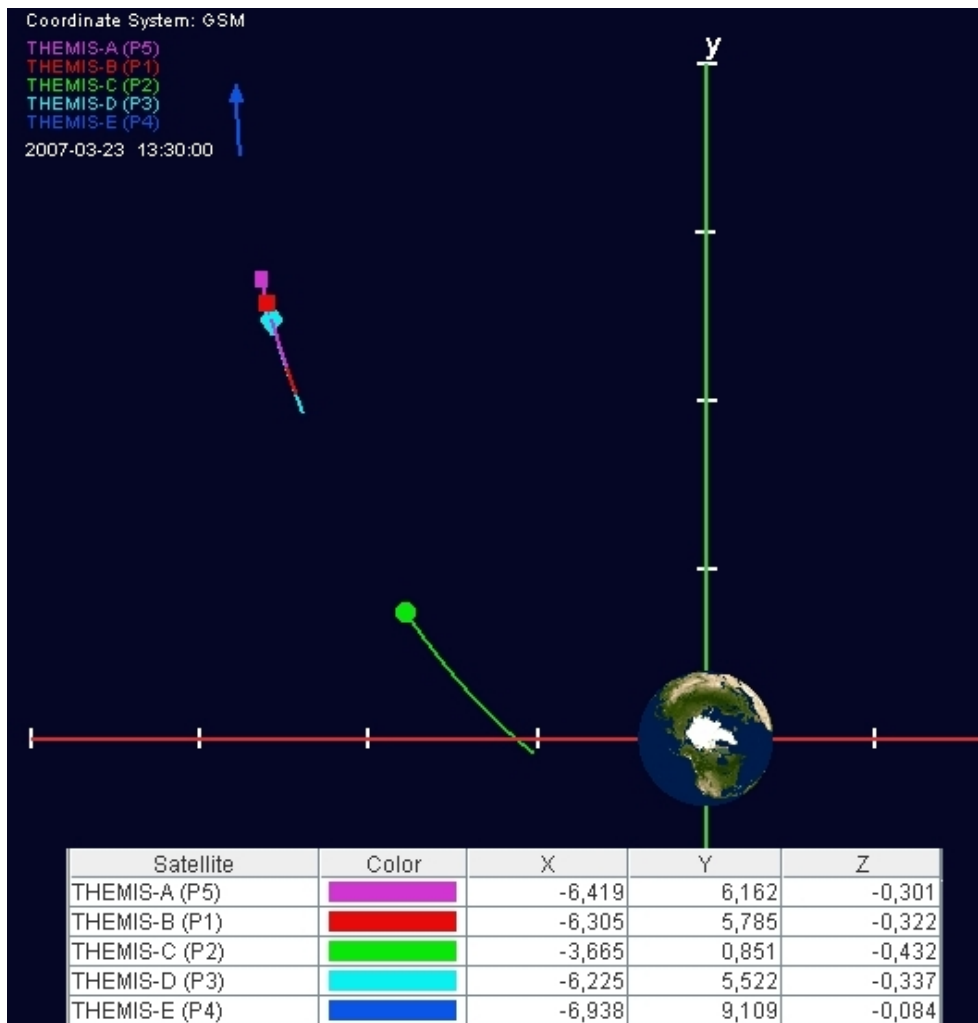


**Fig. 11** THEMIS probe locations (GSM,  $R_E$ ) on Mars 23rd 2007 between 1330 and 1430 UT. Satellite locations are also tabulated in GSM coordinates at 1400 UT

#### 4.4 Substorm event: March 23rd 2007

Two substorms were captured on March 23rd 2007. THEMIS positions are plotted on figure 11 in GSM coordinates between 1330 and 1430 UT around the second local dipolarization. Thc is the leading probe moving from the duskside toward the earth whereas The is the trailing one; Thd, Thb and Tha are in between following Thc in this order. During this period THEMIS constellation is located in the south hemisphere. The first local dipolarization is observed by Thc at 1114:30 UT while ground based observations and Polar data indicate an auroral substorm onset at 1113 UT downward of the mapped point of Thc. This first dipolarization is analyzed in details in [1]. The order of the probe positions is the same as for the second dipolarization displayed figure 11 and discussed later; THEMIS constellation was also located in the dusk side but farther from the earth than during the second event, slightly

closer to the equator. Here we just show a summary plot around the first local dipolarization onset (figure 12) to be able to compare with the second event discussed later in more details. On panel a, the Bz component of the magnetic field is shown in GSM (FGM data) for the five probes, Thc (green) clearly detects the dipolarization first while Thd (cyan), Thb (red), Tha (magenta) and The (blue) detect it later. The delays ( $\simeq 67$  sec) between Thd and The ( $\Delta Y_{d-e} \simeq 2.5 R_E$ ) calculated from both Bz, from Vx or from Vy signatures (panel j) give an estimated azimuthal propagation velocity of about 240 km/s. It agrees also with the velocity inferred from ground based and polar observations (for more details see [1]). ULF Magnetic fluctuations amplitudes (panel b) as well as integrated powers (panel h) recorded by SCM in the range 0.45 to 4 Hz (scf data) increase at the dipolarization and are well correlated with the amplitude of the x component of the ion velocity (panel i). Most of the ULF magnetic activity is below 4 Hz (panels c,d,e,f,g) and around the proton cyclotron frequency ( $f_{c,i} \simeq 0.6$  Hz). Note that a high level of spurious noise below 1.5 Hz is still present despite of the cleanup process; it is due to particular conditions during the commissioning on March 23rd. The ion velocity increases suddenly at the dipolarization especially on the Vx component up to 350 km/s on Thc and Thd (panel i).

Now we deal with the second dipolarization which starts first at 1358:30 UT on Thd. Fortunately this dipolarization is caught by the THEMIS constellation during a particle burst period. Unfortunately POLAR cameras were not in a position to detect it. Figure 13 displays an overview of Tha data on March 23rd between 1330 and 1430 UT during a fast survey period. Panels a,b, and c show that the magnetotail is stretching from 1330 to 1358:30 UT, as expected for a growth phase; the Bx and By components are increasing in modulus (from 25 nT to 33 nT, and from 35 nT to 55 nT, respectively). Remind that the THEMIS constellation is located in the dusksector therefore both Bx and By correspond to the components of the magnetotail. The dipolarization occurs suddenly at 1359 UT as Bz increases from 3 nT to 10 nT and By decreases from 55 nT to 45 nT. Magnetic low-frequency fluctuations are recorded (5-15 mHz) until the end of the dipolarization around 1410 UT when the Bz component reaches 16 nT while By  $\simeq 35$  nT. Panel e (SST data) and panels f,h, and i (ESA data) indicate that the ions are mostly accelerated and heated at the dipolarization onset while electrons seem to be accelerated in successive steps (panels j and k). Panel g shows a short lasting peak in the ion density profile at the beginning of the dipolarization onset and panel h gives evidence for low-frequency fluctuations on the three components of the velocity. Note that the oscillation on the Vy component of the ion velocity starts before the dipolarization. Finally panels m, n, l, and o show four intensifications of magnetic fluctuations during the dipolarization. Again most of the ULF magnetic fluctuations are below 4 Hz and around  $f_{c,i} \simeq 0.64$  Hz. Figure 14 is a zoom on the dipolarization period data gathered by Tha (magenta), Thb (red), Thd (cyan) and The (blue). Thc is too close to the earth and misses the dipolarization. Panel a shows that the increase of the Bz component starts first on Thd ( $\simeq 1358:30$  UT), then Thb ( $\simeq 1358:50$  UT), Tha ( $\simeq 1359:00$  UT) and finally on The ( $\simeq 1400:20$  UT). The delay ( $\simeq 110$  sec) between Thd and The ( $\Delta Y_{d-e} \simeq 3.6 R_E$ ) calculated from both Bz signatures give an estimated azimuthal propagation velocity of about 210 km/s; the same estimation using Tha and The gives 240 km/s. Panel b shows SCM Bz waveforms which give the same timing for the dipolarization onset. Note that the largest Bz amplitudes (SCM data) correspond to successive local dipolarizations (FGM data). Panels c,d,e and f indicate for each probe (in the observed order of the dipolarization Thd, Thb, Tha and The) that the power spectral density increases suddenly at the dipolarization and is again maximum for fluctuations with frequencies below 4 Hz. Integrated power of the magnetic fluctuations between 0.45 and 4 Hz is plotted on panel g. These integrated powers are smaller ( $\simeq 5 \cdot 10^{-3} - 3 \cdot 10^{-2} \text{ nT}^2$ ) than those recorded closer to the magnetic equator

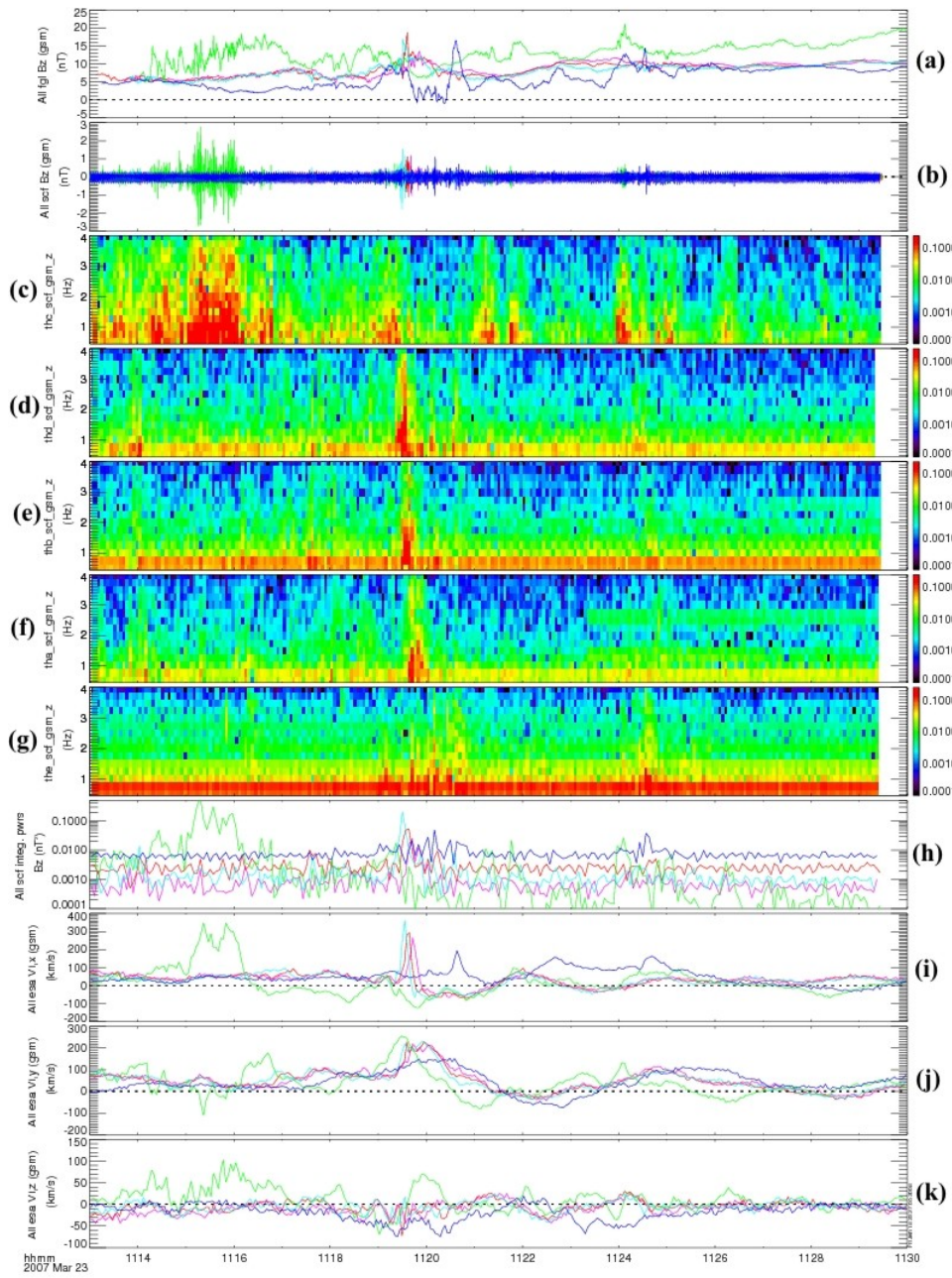


**Fig. 12** Five THEMIS probes data in fast survey mode on March 23rd 2007 between 1113 and 1130 UT. From top to bottom Panel a: Bz from FGM data with 0.5 sec of time resolution, panel b: Bz from SCM waveform data between 0.45 to 4 Hz, panels c (The),d (Thd),e (Thb),f (Tha),g (The): SCM Bz power spectral densities, panel h: integrated powers from 0.45 to 4 Hz with 4 sec of time resolution for the 5 probes, panels i,j,k: x,y, and z components of the ion velocity with 3 sec of time resolution.

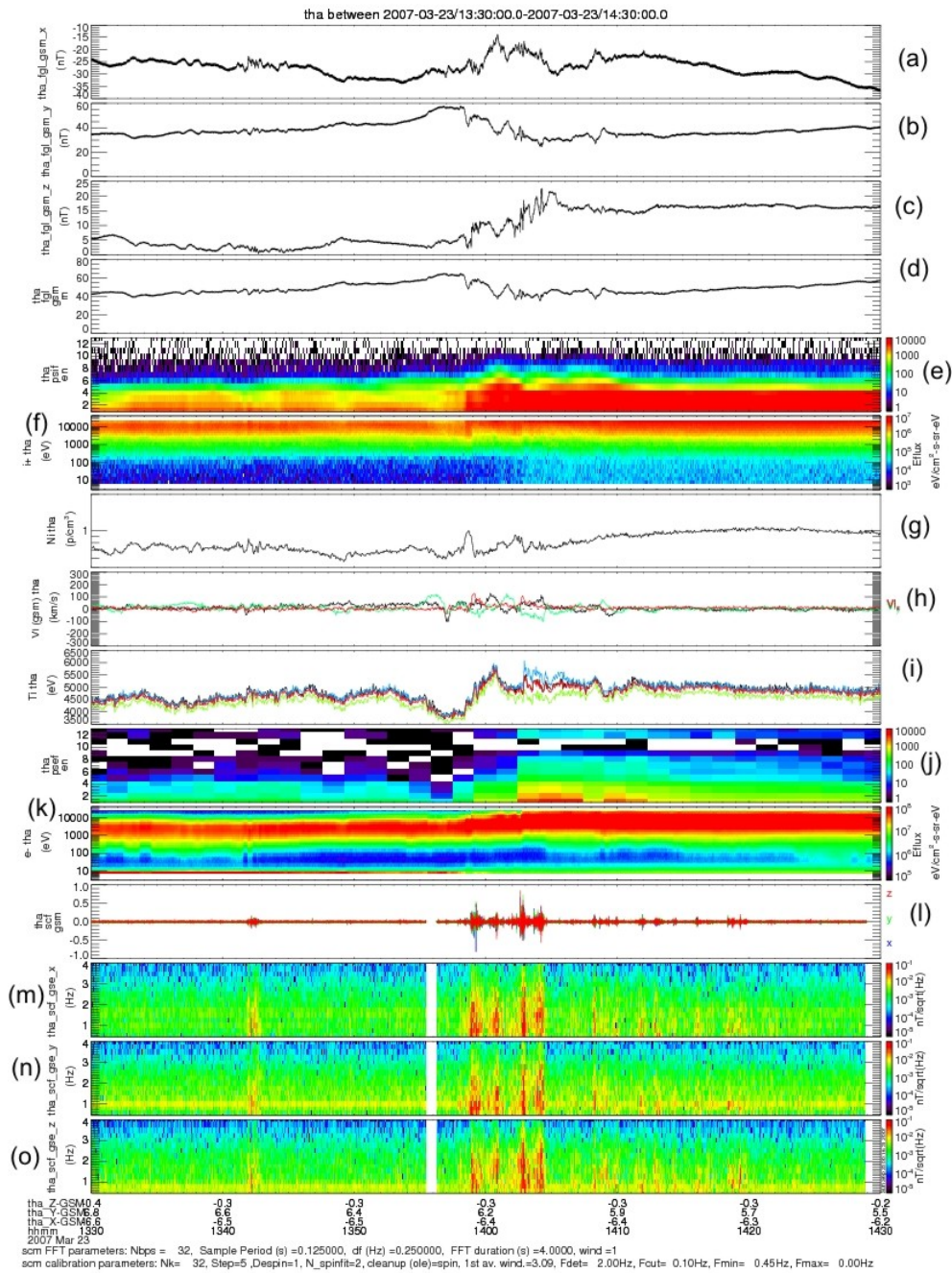


**Fig. 13** Overview of Tha (fast survey) data on March 23rd 2007 between 1330 and 1430 UT. From top to bottom:  $B_x$ ,  $B_y$ ,  $B_z$  and  $B$  (FGM data), ion energy spectrograms (SST and ESA data), density, velocity and temperature, electron energy spectra (SST and ESA data), waveform and spectrograms of magnetic fluctuations from 0.45 Hz to 4 Hz, (SCM data)

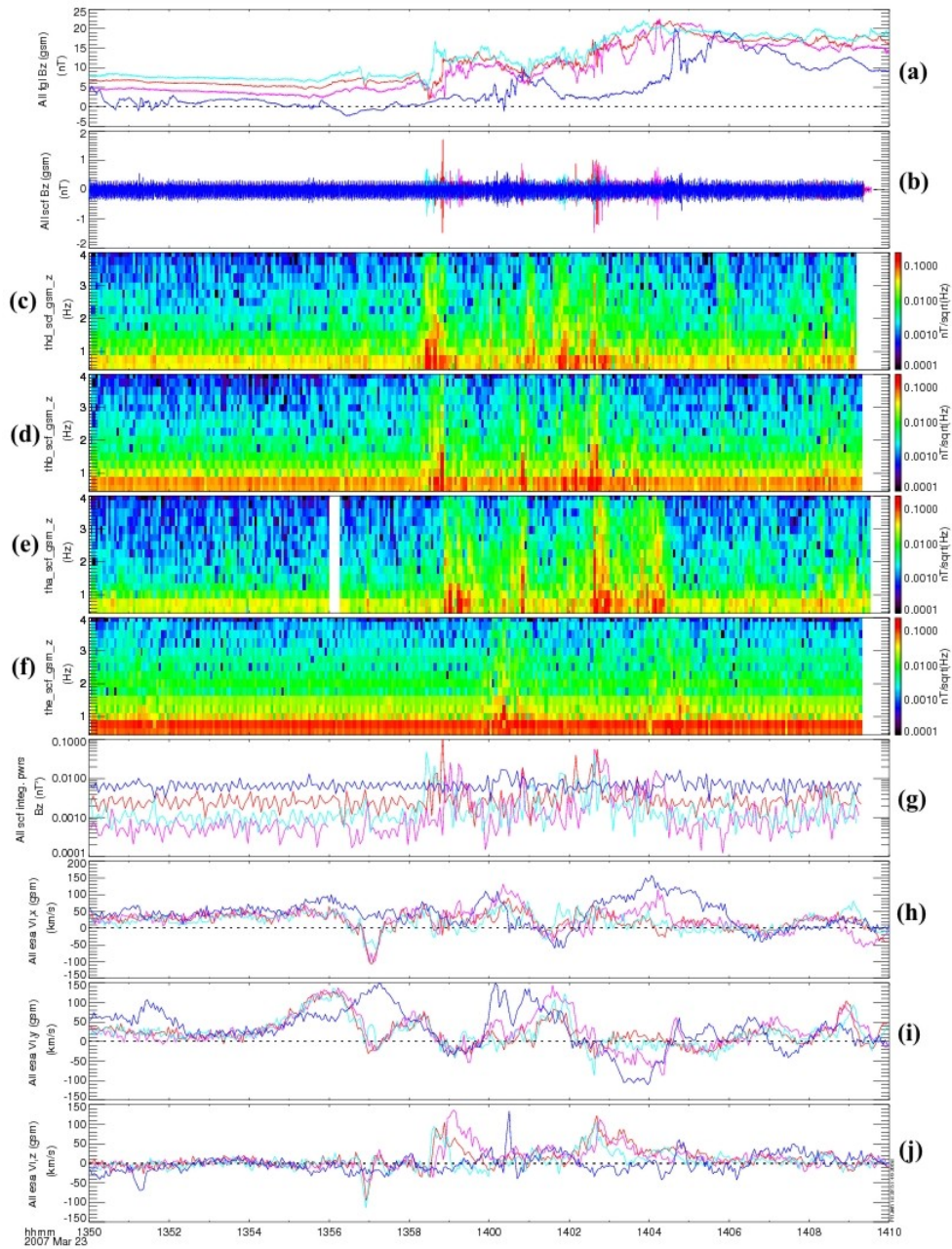


**Fig. 14** Four THEMIS probes (a, b, d, and e) data from fast survey mode on March 23rd 2007 between 1350 and 1410 UT. Panel a: Bz from FGM data with 0.5 sec of time resolution, panel b: Bz from SCM data from 0.45 to 4 Hz, panels c (Thd),d (Thb),e (Tha),f (The): SCM Bz power spectral densities and panel g: integrated powers from 0.45 to 4 Hz with 4 s time resolution, panels h,i,j: x,y, and z components of the ion velocity with 3 sec time resolution.

at the geostationary orbit (see for instance [22, 14]). They are poorly correlated with the velocity profiles shown in the next panels as compared with the first dipolarization. It could be due to the fact that all probes are farther from the source of the waves. The last panels (i,j,k) show the three components of the ion velocity. Amplitudes are smaller than for the first event. These lower velocities may be due to an underestimate of the velocities by ESA (see [21] for more details). Indeed the ion energy exceeds 40 keV, the upper energy limit of ESA and clearly enters in the energy range of the SST instrument (see panels e and f on figure 13). While the first dipolarization onset is characterized mainly by a large  $V_x$  component up to 350 km/s, the second one has a different signature: large values of the  $V_z$  component at the dipolarization onset (panel k). These large  $V_z$  values toward the magnetic equator are recorded in the same order as the dipolarization (Thd, Thb, and Tha) and could be interpreted as the motion of the magnetic field lines toward the earth during the dipolarization. Figure 15 is the same as Figure 14 but for particle burst period during 1358:10 and 1402:00 UT. Therefore time resolutions are better for magnetic field data (FGM as well as SCM at 128 S/s). We observe the same signatures: dipolarization on Thd, Thb, Tha and The (panel a), ULF/ELF magnetic fluctuations now up to 64 Hz but maximum intensities still below 4 Hz (panels b,c,d,e and f), integrated power up to  $3 \cdot 10^{-2}$  (panel g), large ion  $V_z$  at the dipolarization onset (panel k). Again the integrated power of magnetic fluctuations is somewhat smaller than previously reported values from geostationary spacecraft. Note that no intense wave emission is recorded around  $f_{LH} \simeq 27$  Hz, the lower hybrid frequency which is well included in the range of SCM, in the scp mode. Finally we can remark that the SCM spectra performed from wave burst data shown in figure 3 are taken during this substorm period (135946-140016 UT). However the level of measured noise is similar to NEMI measured at ground. Therefore we can conclude that at least during this short lasting period no high-frequency waves are emitted notably in the range of whistler waves (between  $f_{c,i} \simeq 0.7$  Hz to  $f_{c,e} \simeq 1.4$  kHz).

## 5 Summary and conclusions

SCM and EFI are designed to characterize electromagnetic fluctuations at substorm onset and to clarify their role in the different phases of the substorm expansion. We described the calibration method for the SCM instrument, as well as the cleanup process which allows to recover the sensitivity of the SCM instrument, as it was measured on the ground. First THEMIS SCM results, obtained in various regions, from the solar wind to the magnetotail, were presented and discussed. The usefulness of the magnetic fluctuations for the identification of the key regions of the magnetosphere was discussed. Their possible role in the different basic plasma processes was pointed out. Notably it was suggested that ULF fluctuations could heat electrons inside an FTE event (May 20, 2007). It has been shown that the level of the ULF magnetic fluctuations mostly below 4 Hz (around  $f_{c,i}$ ) during substorms (March 23rd, 2007, 1113 and 1358 UT) is largely enhanced during the dipolarization associated with these substorms. These first THEMIS SCM results demonstrate that the 5 tri-axis instruments function perfectly, and illustrate the capability of the THEMIS mission to provide a comprehensive set of data not only on substorms but also on the physics of key regions such as magnetopause and bow shock

**Acknowledgements** We are pleased to acknowledge the friendly collaboration and the help of other THEMIS team members, in particular, P. Harvey, R. Jackson, J. Lewis, M. Ludlam, D. Meilhan, H. Richard, and E.

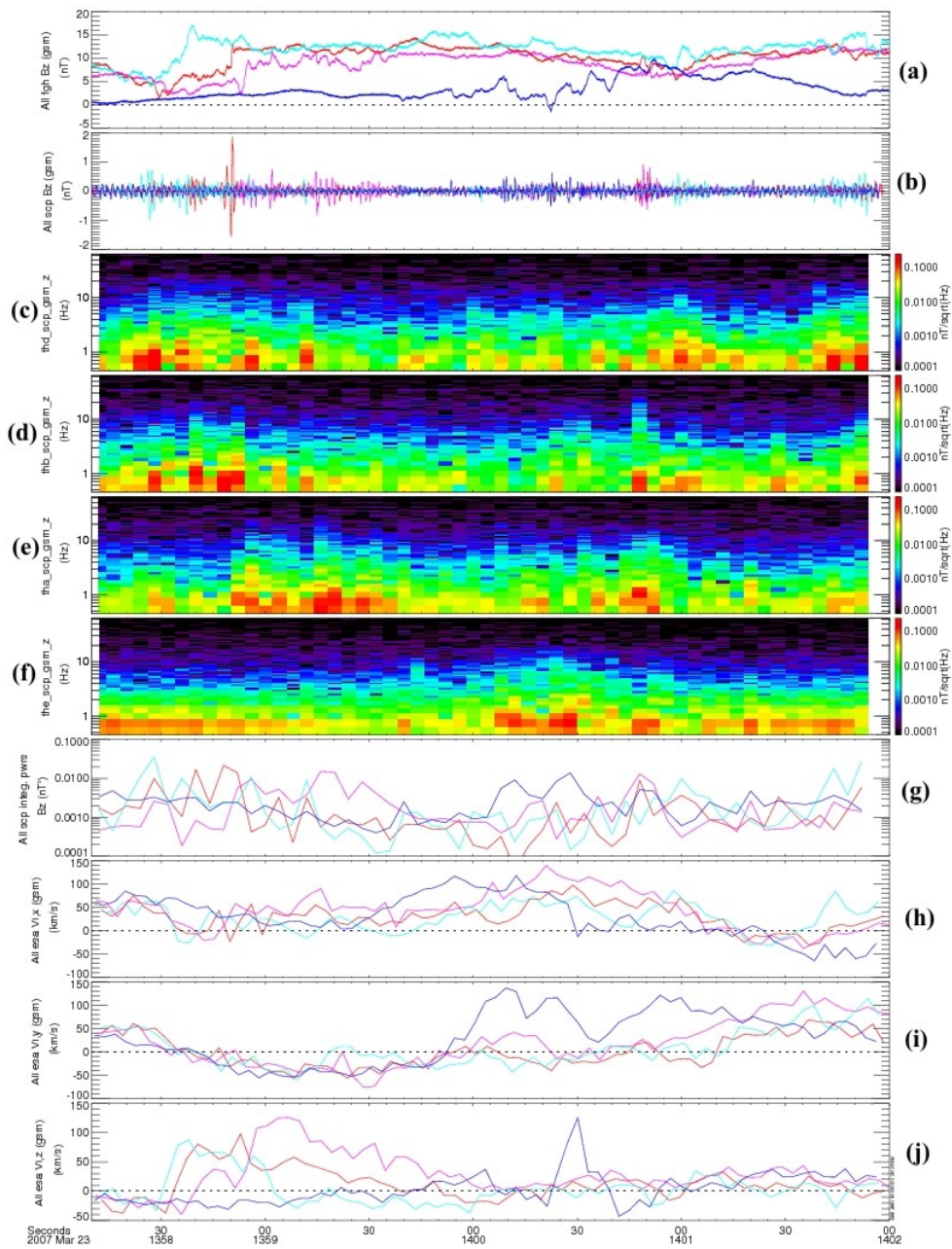


**Fig. 15** Four THEMIS probes (a, b, d, and e) data from particle burst mode on March 23rd 2007 between 1358:10 and 1402:00 UT. Panel a: Bz from FGM data sampled at 128 S/s, panel b: Bz from SCM data at 128 S/s filtered between 0.45 and 64 Hz, panels c (Thd),d (Thb),e (Tha),f (The): SCM Bz power spectral densities, and panel g: integrated powers from 0.45 to 64 Hz with 4 sec of time resolution, panels h,i,j: x,y and z components of the ion velocity with 3 sec of time resolution.

Taylor. The French involvement on THEMIS is supported by CNES and CNRS. Work in the US was supported by NASA contract NAS5-02099

## References

1. Angelopoulos, V.*et al.*: The THEMIS mission. *Space Science Review* **this issue** (2008)
2. Attico, N., Califano, F., Pegoraro, F.: Kinetic regimes of high frequency magnetic reconnection in a neutral sheet configuration. *Phys. Plasmas* **9**, 458–464 (2002)
3. Auster, H.U., Glassmeier, K.H., Magnes, W., Aydogar, O., Baumjohann, W., Constantinescu, D., Fischer, D., Fornacon, K.H., Georgescu, E., Harvey, P., Hillenmaier, O., Kroth, R., Ludlam, M., Narita, Y., Nakamura, R., Okrafka, K., Plaschke, F., Richter, I., Schwarzl, H., Stoll, B., Valavanoglou, A., Wiedemann, M.: The THEMIS fluxgate magnetometer. *Space Science Review* **this issue** (2008)
4. Bonnell, J.*et al.*: Electric field instrument for THEMIS. *Space Science Review* **this issue** (2008)
5. Bulanov, S.V., Pegoraro, F., Sakharov, A.S.: Magnetic reconnection in electron dynamics. *Phys. Fluids B* **4**, 2499–2508 (1992)
6. Cheng, C.Z., Lui, A.T.Y.: Kinetic ballooning instability for substorm onset and current disruption observed by AMPTE/CCE. *Geophys. Res. Lett.* **25**, 4091 (1998)
7. Cornilleau-Wehrlin, N. and G. Chanteur and S. Perraut and L. Rezeau and P. Robert and A. Roux and C. de Villedary and P. Canu and M. Maksimovic and Y. de Conchy and D. Hubert and C. Lacombe and F. Lefeuvre and M. Parrot and J.-L. Pinçon and P. M. E. Décréau and C. C. Harvey and P. Louarn and O. Santolik and H. St. Alleyne and M. Roth and T. Chust and O. Le Contel and STAFF team: First results obtained by the Cluster STAFF experiment. *Annales Geophysicae* **21**, 437–456 (2003)
8. Gendrin, R.: Substorm aspects of magnetic pulsations. *Space Science Reviews* **11**, 54–130 (1970)
9. Gurnett, D.A., Frank, L.A., Lepping, R.P.: Plasma waves in the distant magnetotail. *J. Geophys. Res.* **81**, 6059–6071 (1976)
10. Karpman, V.I., Meerson, B.I., Mikhailovsky, A.B., Pokholetov, O.A.: *Planet. Space Sci.* **25**, 273 (1977)
11. Krasnosselskikh, V.V., Lembège, B., Savoini, P., Lobzin, V.V.: Nonstationarity of strong collisionless quasiperpendicular shocks: Theory and full particle simulations. *Physics of Plasma* **9**, 1192–1209 (2003)
12. Kremser, G., Korth, A., Ullaland, S.L., Perraut, S., Roux, A., Pedersen, A., Schmidt, R., Tanskanen, P.: Field-aligned beams of energetic electrons (16 keV <E<80 keV) observed at geosynchronous orbit at substorm onsets. *J. Geophys. Res.* **93**, 14,453 (1988)
13. Le Contel, O., Perraut, S., Roux, A., Pellat, R.: Plasma transport during growth phase and relation to breakup during substorm growth phase and relation to breakup. *Space Science Reviews* **95**, 415–426 (2001)
14. Le Contel, O., Roux, A., Perraut, S., Pellat, R., Holter, Ø., Pedersen, A., Korth, A.: Possible control of plasma transport in the near-earth plasma sheet via current-driven Alfvén waves ( $f \approx f_{H^+}$ ) during substorm growth phase and relation to breakup. *J. Geophys. Res.* **106**, 10,817–10,827 (2001)
15. Le Contel, O., Roux, A., Perraut, S., Pellat, R., Robert, P., Chanteur, G., Fontaine, D., Cornilleau-Wehrlin, N., Sauvaud, J.A., Cully, C., Parks, G., Chua, D., André, M., Balogh, A., Fazakerley, A., Rème, H., Nagai, T., Mukai, T., Hayakawa, H., Matsuoka, A., Anderson, R.R., Matsumoto, H.: Role of the parallel current instability during substorms: Theory and observations. In: R. Winglee (ed.) *Sixth International Conference on Substorms(ICS-6)*, March 25-29, 2002, pp. 326–333. University of Washington, Seattle (2002)
16. Le Contel, O., Sahraoui, F., Roux, A., Fontaine, D., Robert, P., Sauvaud, J.A., Owen, C., Fazakerley, A.N.: Small scale cluster observations of current sheet disruptions during substorms. In: M. Syrjaeso, E. Donovan (eds.) *Eighth International Conference on Substorms (ICS-8)*, March 27-31, 2006, pp. 143–148. University of Calgary, Canada (2006)
17. Ludlam M., *et al.*: The THEMIS magnetic cleanliness program. *Space Science Review* **this issue** (2008)
18. Lui, A.T., Lopez, R.E., Anderson, B.J., Takahashi, K., Zanetti, L.J., McEntire, R.W., Potemra, T.A., Klumpar, D.M., Greene, E.M., Strangeway, R.: Current disruption in Earth’s magnetosphere: Observations and models. *J. Geophys. Res.* **101**, 13,067–13,088 (1996)
19. Lui, A.T.Y., Chang, C.L., Mankofsky, A., Wong, H.K., Winske, D.: A cross-field current instability for substorm expansions. *J. Geophys. Res.* **96**, 11,389–11,401 (1991)
20. Mandt, M.E., Denton, R.E., Drake, J.F.: Transition to whistler mediated magnetic reconnection. *Geophys. Res. Lett.* **21**(1), 73–77 (1994)
21. McFadden, J.P., Carlson, C.W., Larson, D., Angelopoulos, V.: THEMIS ESA first science results and performance issues. *Space Science Review* **this issue** (2008)
22. Perraut, S., Le Contel, O., Roux, A., Pedersen, A.: Current-driven electromagnetic ion cyclotron instability at substorm onset. *J. Geophys. Res.* **105**, 21,097–21,107 (2000)

- 
23. Perraut, S., Le Contel, O., Roux, A., Pellat, R., Korth, A., Holter, Ø., Pedersen, A.: Disruption of parallel current at substorm breakup. *Geophys. Res. Lett.* pp. 4041–4044 (2000)
  24. Perraut, S., Morane, A., Roux, A., Pedersen, A., Schmidt, R., Korth, A., Kremser, G., Aparicio, B., Pellinen, R.: Characterization of small scale turbulence observed at substorm onsets: Relationship with parallel acceleration of particles. *Adv. Space Res.* **13(4)**, 217 (1993)
  25. Quinn, T., Bonnell, J.W., Roux, A., Auster, U., Larson, D., Khurana, K., Ludlam, M., Harvey, P., Angelopoulos, V.: THEMIS Science Coordinate Systems Definition THM-SOC-110 Sept. 29, 2006 (2006)
  26. Rezeau, L., Belmont, G.: Magnetic turbulence at the magnetopause, a key problem for understanding the solar wind/magnetosphere exchanges. *Space Science Reviews* **95**, 427–441 (2001)
  27. Robert, P., Gendrin, R., Perraut, S., Roux, A., Pedersen, A.: Geos-2 identification of fastly moving current structures in the equatorial outer magnetosphere during substorms. *J. Geophys. Res.* **89**, 819 (1984)
  28. Roux, A., Le Contel, O., Robert, P., Coillot, C., Bouabdellah, A., la Porte, B., Alison, D., Ruocco, S., Vassal, M.C.: The Search Coil Magnetometer (scm) for THEMIS. *Space Sci. Rev.* **this issue** (2007)
  29. Russel, C.T.: Noise in the geomagnetic tail. *Planet. Space Sci.* **20**, 1541–1553 (1972)
  30. Sahraoui, F., Pinçon, J.L., Belmont, G., Rezeau, L., Cornilleau-Wehrin, N., Robert, P., Mellul, L., Bosqued, J.M., Balogh, A., Canu, P., Chanteur, G.: ULF wave identification in the magnetosheath: The k-filtering technique applied to Cluster II data. *J. Geophys. Res.* **108**, 1335 (2003). DOI 10.1029/2002JA009587
  31. Shinohara, I., Nagai, T., Fujimoto, M., Terasawa, T., Mikai, T., Tsuruda, K., Yamamoto, T.: Low-frequency electromagnetic turbulence observed near the substorm onset site. *J. Geophys. Res.* **103**, 20,365 (1998)
  32. Shiokawa, K., Miyashita, Y., Shinohara, I., Matsuoka, A.: Decrease in  $B_z$  prior to the dipolarization in the near-Earth plasma sheet. *J. Geophys. Res.* **110**, A09,219 (2005). DOI 10.1029/2005JA011144
  33. Sibeck, D.G., Angelopoulos, V.: THEMIS science objectives and mission phases. *Space Science Review* **this issue** (2008a)
  34. Sibeck, D.G.*et al.*: *Geophys. Res. Lett.* **this issue** (2008b)
  35. Sigsbee, K., Cattell, C.A., Mozer, F.S., Tsuruda, K., Kokubun, S.: Geotail observations of low-frequency waves from 0.001 to 16 hz during the november 24, 1996, geospace environment modeling substorm challenge event. *J. Geophys. Res.* **106**, 435–445 (2001)
  36. Zhang, Y., Matsumoto, H., Kojima, H.: Whistler mode waves in the magnetotail. *J. Geophys. Res.* **104**, 28,633–28,644 (1999)